Solar Physics manuscript No.
(will be inserted by the editor)

Ionospheric Disturbances and their Impact on IPS Using MEXART Observations

M. Rodríguez-Martínez · H. R. Pérez-Enríquez · A. Carrillo-Vargas · R. López-Montes · E. A. Araujo-Pradere · G. A. Casillas-Pérez · J. A. L. Cruz-Abeyro

Received: date / Accepted: date (will be inserted by the editor)
DOI: 10.1007/s11207-014-0496-8.

arXiv:1402.2490v1 [physics.space-ph] 11 Feb 2014

Abstract We study the impact of ionospheric disturbances on the Earth's environment caused by the solar events that occurred from 20 April to 31 May 2010, using observations from the *Mexican Array Radio Telescope* (MEXART). During this period of time, several astronomical sources presented fluctuations in their radio signals. Wavelet analysis, together with complementary information such as the vertical total electron content (*vTEC*) and the *Dst* index, were used to identify and understand when the interplanetary scintillation (IPS) could be contaminated by ionospheric disturbances (IOND). We find that radio signal perturbations were sometimes associated with IOND and/or IPS fluctuations; however, in some cases, it was not possible to clearly identify their origin. Our Fourier and wavelet analyses

M. Rodríguez-Martínez
Universidad Nacional Autónoma de México, Escuela Nacional de Estudios Superiores, Unidad Morelia. Antigua Carretera a Pátzcuaro No. 8701, Ex-Hacienda de San José de la Huerta. C.P. 58190. Morelia Michoacán, México.

H. R. Pérez-Enríquez
Universidad Nacional Autónoma de México, Centro de Geociencias, Campus Juriquilla. Blvd Juriquilla 3001, Juriquilla Querétaro. 76230, México.

A. Carrillo-Vargas
Universidad Nacional Autónoma de México, Instituto de Geofísica, Unidad Michoacán. Antigua Carretera a Pátzcuaro No.8701, Ex-Hacienda de San José de la Huerta. C.P. 58190. Morelia Michoacán, México.

R. López-Montes
Universidad Nacional Autónoma de México, Centro de Geociencias Campus Juriquilla. Blvd Juriquilla 3001, Juriquilla, Querétaro. 76230, México.

E. A. Araujo-Pradere
CIRES-University of Colorado. 325 Broadway W/NP9. Boulder, CO, USA.

G. A. Casillas-Pérez
Universidad Nacional Autónoma de México, Instituto de Geofísica, Unidad de Cómputo. Ciudad Universitaria, C.P. 04510, México.

J. A. L. Cruz-Abeyro
Universidad Nacional Autónoma de México, Centro de Geociencias, Campus Juriquilla. Blvd Juriquilla 3001, Juriquilla Querétaro. 76230, México.
E-mail: mrodriguez@enesmorelia.unam.mx

showed that these fluctuations had frequencies in the range $\approx 0.01\,\mathrm{Hz}$ – $\approx 1.0\,\mathrm{Hz}$ (periodicities of 100 s to 1 s).

Keywords Interplanetary scintillation · Ionospheric disturbances · MEXART · *vTEC*

1 Introduction

Large-scale solar-wind disturbances in the interplanetary medium (IPM) can, and frequently do, distort radio-wave fronts coming from compact radio sources producing the so-called interplanetary scintillation (IPS) (Hewish, Scott, and Wills, 1964; Hewish and Bravo, 1986). It is known that radio sources with an angular diameter smaller than 1 arcsec present interplanetary scintillation at frequencies $> 0.1\,\mathrm{Hz}$ (Hewish and Duffet-Smith, 1987); though, depending on the observing wavelength, IPS can be present beyond 10 Hz (Milne, 1976; Manoharan and Ananthakrishnan, 1990; Manoharan, Kojima, Misawa, 1994; Manoharan, 2010). IPS on a large number of compact radio sources has been observed using the *Ooty Radio Telescope* (ORT), *Solar-Terrestrial Environment Laboratory* (STEL) and *Mexican Array Radio Telescope* (MEXART), providing insight on solar-wind properties (Manoharan and Ananthakrishnan, 1990; Manoharan, Kojima, Misawa, 1994; Mejia-Ambriz et al., 2010).

Solar events can affect the plasma of the Earth's ionosphere either directly, through X-ray and/or EUV radiation from flares as it reaches Earth, or indirectly, through the perturbation of the magnetospheric electric field upon the arrival of an interplanetary CME (Tsurutani et al., 2009). The Earth's ionosphere is considered a dispersive medium for radio waves. Its refractive index is a function of the radio-wave frequency, the electron density, and the intensity of the Earth's magnetic field, **B**. Its perturbation can be an important source of error for the signals of the *Navstar Global Positioning System* (GPS) satellites and other positioning systems like *Galileo* (European Union), *Glonass* (Russia), and *Compass* (China). The error in the signals is proportional to the integrated electron density along the signal path, TEC, and inversely proportional to the square of the carrier phase frequency, $\tau \propto TEC/\nu^2$ (Langley, 1996; Komjathy, 1997). The signals from GPS satellites must travel through the Earth's ionosphere in their way to the GPS receivers (on the Earth's surface) in the L-band: $L_1 = 1575.42\,\mathrm{MHz}$ and $L_2 = 1227.60\,\mathrm{MHz}$. Although there is another L-band, $L_3 = 1381.05\,\mathrm{MHz}$, GPS users cannot use it (Erickson et al., 2001).

Several works have shown the importance of the ionospheric interference on the IPS (Gapper et al., 1982; Purvis et al., 1987; Tappin et al., 1984; Woan, 1995; Lucek et al., 1996; Jackson et al., 1998; Pérez-Enríquez et al., 2008; Shishov et al., 2010). Part of this contamination, or ionospheric scintillation (IONS), can represent a serious problem in IPS studies. In fact, the presence of IONS can lead to a misinterpretation of the IPS; however, there are techniques to remove the ionospheric scintillation part. Carrillo-Vargas et al. (2012) have explored another possible data contamination by ionospheric effects. They have shown an example related to a solar event on 15 December 2006, where the fluctuations observed in the signal of the radio sources exhibited strong contamination by ionospheric disturbances (IOND). The behavior shown by the radio signal was consistent with the fluctuations observed from the signal emitted by polar satellites. The authors

suggested that not only the total electron content (TEC) and the geomagnetic equatorial index, *Dst*, could be used to characterize the origin of such fluctuations, but also the possibility of removing the contaminating frequencies from the data to study separately the IPS or the IOND.

Since we have observed fluctuations in the radio signal of sources transiting the MEXART observatory, the purpose of our study is to understand the nature of these fluctuations, as well as answering the following questions: Are the fluctuations intrinsic to quiet solar-wind conditions? When are these fluctuations related to ionospheric disturbances? How do these fluctuations quantitatively affect the IPS? To answer these questions, we have analyzed the radio signal of sources observed with the MEXART. We have explored all observations to find if the ionospheric contribution is always present, even in the absence of solar events. In Section 2, we present the information related to the MEXART observations for the period between April and May 2010. Section 3 shows the data analysis applied and the results using wavelet analysis applied to the MEXART data. Finally, in Sections 4 and 5 we present the discussion and conclusions of our work, respectively.

2 Observations

We considered two short periods of MEXART (located at a latitude of $+19^\circ\ 48'\ 39''$, longitude of $-101^\circ\ 41'\ 39''$, and elevation of 1964 m above mean sea level) observations, from 20 to 30 April and 8 to 31 May 2010, with a configuration that used a small section of the MEXART antenna. We used a 1024-dipole rectangular sub-array arranged in 16 rows. Each row is horizontally polarized in the East-West direction. The total area of the antenna is 2415 square meters, 17.25 m (North-South) $\times$ 140 m (East-West), which is one fourth of the total MEXART array. The array feeds a 16x16 Butler matrix, which generates 16 beams, each of width 1x8 degrees. The receiver works at 139.65 MHz with a 2 MHz bandwidth and a time constant of 40 ms. The acquisition rate is 20 ms. Further technical details of the radio telescope can be found elsewhere (González-Esparza et al., 2004, 2006; Carrillo-Vargas, 2007). The daily MEXART observations and the transit of strong radio sources can be viewed in real time[1].

Transit observations of the following sources were taken on several days: 3C48 (R. A. $= 01^h37^m41.3^s$, Dec $= +33^\circ09^m35^s$, right ascension and declination respectively), 3C144 (R. A. $= 05^h\ 34^m\ 32.0^s$, Dec $= +22^\circ\ 00^m\ 52^s$), 3C274 (R. A. $= 12^h\ 30^m\ 49.4^s$, Dec $= +12^\circ\ 23^m\ 28^s$), Cas A (R. A. $= 23^h\ 23^m\ 27.9^s$, Dec $= +58^\circ\ 48^m\ 42^s$), Cen A (R. A. $= 13^h\ 25^m\ 27.6^s$, Dec $= -43^\circ\ 01^m\ 09^s$), and 3C405 (R. A. $= 19^h\ 59^m\ 28.3^s$, Dec $= +40^\circ\ 44^m\ 02^s$). The coordinates are precessing at equinox J2000.0 and are represented in a map (Figure 1) showing the right ascension (R. A.) and declination (Dec). Table 1 lists the observation dates of the sources whose radio signal presented fluctuations when transiting the MEXART observatory (see first and second columns). We use the MEXART position (latitude, longitude and elevation) and the precessed coordinates (R. A. and Dec) for each radio source to determine their transit time during the date we analyze MEXART data. The third column in Table 1 shows the corresponding elongation

[1] http://www.mexart.unam.mx

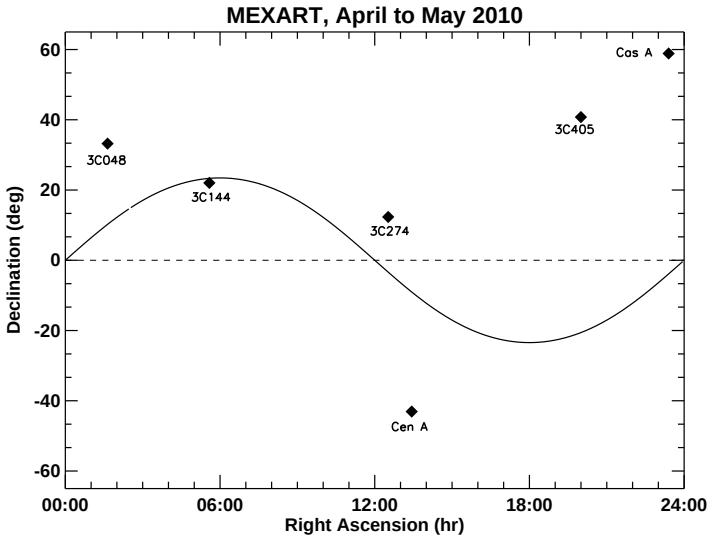

Figure 1 Location of the radio sources observed with MEXART. These radio sources were observed between 20 April and 31 May 2010. The orbit of the Sun along the year is indicated with a continuous line.

angle (ϵ, the angle between the Sun-Earth-line and the source) in degrees for each source. The radio source 3C144 shows the smallest ϵ values, all fluctuations shown by these sources were analyzed to characterize their origin. There are days with no MEXART observations; they appear as blank in Table 1.

2.1 The *vTEC* and the *Dst* index

When analyzing radio sources observed by any telescope, such as MEXART, it is important to take into account the conditions in the environment. The origin of the fluctuations observed in the radio signal of each source can be understood if we analyze them together with the characteristics of the geomagnetic field and the ionosphere. In this context, we included the geomagnetic equatorial *Dst* index (the provisional values from Kyoto[2]) and the vertical total electron content[3] (*vTEC*) to understand the potential correlation between geomagnetic storms and ionospheric disturbances. The ionospheric total electron content is a well suited parameter to study the conditions of the perturbed ionosphere and it is particularly important to correct the positioning information for single-frequency GPS users (Araujo-Pradere, 2005; Araujo-Pradere, Fuller-Rowell, and Spencer, 2006). To facilitate the comparison between the *Dst* index and the *vTEC* properties, in the fourth and fifth column of Table 1, we list the averaged *Dst* index, $< Dst >$, and the corresponding minimum value of *Dst*, Dst_{min}, for each day. Finally, we have included the dispersion of *vTEC*, δ, which is defined as:

[2] `http://wdc.kugi.kyoto-u.ac.jp/dstdir/`

[3] Usually the *vTEC* is measured in *TEC* units (*TECu*), where $1\,TECu = 10^{16}\,\mathrm{m}^{-2}$.

$$\delta = \frac{(vTEC_{max} - < vTEC >)}{< vTEC >}, \quad (1)$$

values of $\delta \gtrsim 4$ indicate that $vTEC$ is strongly disturbed (see for instance López-Montes et al., 2012; Carrillo-Vargas et al., 2012).

Table 1: Sources showing fluctuations in the radio signal observed by MEXART observatory. The δ parameter is the dispersion of $vTEC$ (see Section 2.1).

Date (2010)	Sources	ϵ (°)	$< Dst >$ (nT)	Dst_{min} (nT)	δ
20 April			1	-10	1.50
21 April			1	-7	1.33
22 April			5	-5	1.71
23 April	3C144, 3C405	50.6, 82.6	-9	-22	1.48
24 April	Cas A	55.1	-12	-23	1.47
25 April	3C144, 3C405, Cas A	48.7, 83.6, 55.2	1	-5	1.65
26 April	3C274, Cen A, Cas A	143.7, 148.8, 55.3	7	2	1.23
27 April	3C144, Cas A	46.7, 55.4	5	0	1.33
28 April	3C144, 3C405, Cas A	45.8, 85.1, 55.6	7	-3	1.56
29 April	3C405, Cas A	85.6, 55.7	2	-6	1.55
30 April			0	-4	1.75
7 May			-14	-23	1.35
8 May	3C144	36.1	-8	-28	1.10
9 May			-6	-13	1.41
10 May			4	-8	1.38
11 May	3C274, Cen A	130.2, 146.4	8	-8	1.76
12 May			-8	-12	1.09
13 May			1	-10	1.46
14 May			3	-3	1.97
15 May			-3	-13	1.92
16 May			4	-3	1.72
17 May			-1	-12	2.29
18 May			-3	-28	2.37
19 May	Cas A	60.4	0	-2	1.93
20 May	3C405, Cas A	95.8, 60.7	-12	-17	1.64
21 May	3C405	96.3	3	-11	1.96
22 May	3C405, Cas A	96.8, 61.4	3	-3	1.43
23 May	3C405, Cen A	97.3, 141.0	5	-1	1.16
24 May	3C405	97.7	10	0	1.17
25 May	3C405	98.2	9	0	1.34
26 May	3C405, Cas A	98.7, 62.9	-4	-4	1.57
27 May	Cas A	63.3	1	-3	1.45
28 May	3C144, 3C405, Cas A	16.7, 99.6, 63.7	-3	-3	1.52
29 May	3C144, 3C405, Cas A	16.0, 100.1, 64.1	-29	-85	1.28
30 May			-37	-48	1.93
May 31			-32	-37	1.34

Table 2 Location of the GPS-signal recording stations used to calculate the *vTEC*. The fifth column corresponds to the elevation above sea level of each station.

Monument Name	Monument Code	Latitude (N)	Longitude (W)	Elevation (m)
Coeneo	UCOE	19° 48′ 47″	101° 41′ 39″	1978.8
Celaya	CEGA	20° 31′ 40″	100° 48′ 55″	1750.0
Aguascalientes	INEG	21° 51′ 22″	102° 17′ 03″	1888.4
Oaxaca	OAX2	17° 04′ 42″	96° 43′ 00″	1607.3
Toluca	TOL2	19° 37′ 35″	99° 38′ 36″	2651.9

The *vTEC* values reported here were calculated using five GPS receivers in stations that cover a wide region of the sky and that were located in the proximity of the MEXART observatory: Coeneo (UCOE), Celaya (CEGA), Aguascalientes (INEG), Oaxaca (OAX2) and Toluca (TOL2). Table 2 shows the location (latitude and longitude) and the elevation of the GPS-signal recording stations.

3 Data Analysis and Results

The data analysis was done in two steps: first we analyze MEXART data and second we study the ionospheric data.

3.1 MEXART Data

Data analysis of MEXART radio signals yielded two statistical parameters: the signal to noise ratio (S/N) and the average root mean square (rms) value calculated for the previous and the ensuing days for each radio source observational period. We analyzed the time series for each source transit-time (around 8 minutes), looking for strong fluctuations in the radio signals.

We used several routines developed to analyze MEXART data in which we included one to read the raw data, another one to remove interference and gaps, and a third one that included gaussian fits to obtain a detrended time series.

The time interval covered by the GPS data was the same, 20 April to 31 May, 2010. During this period, the GPS data showed the typical diurnal variation without any significant event. However, the *vTEC* showed a maximum of about 30 *TECu* associated with the geomagnetic storm with a minimum Dst of -85 nT, which occurred on 29 May. Figure 2 shows the *vTEC* for each station, where the *vTEC* series is given every 15 minutes. The lower panel in Figure 2 shows the evolution of the *Dst* index. We observe two minima, one around 2 May (with a minimum value of -67 nT at 18:00 UT) and a second one on 29 May (with a minimum value of -85 nT between 13:00 and 14:00 UT).

The two minima, mentioned above, were probably associated with the coronal mass ejections (CME[4]) that occurred in active regions 11063 and 11072, or with the coronal holes located close to central meridian around four days before they were registered. These solar events certainly modified the plasma conditions in

[4] See the Large Angle and Spectroscopic (LASCO) CME catalog at `http://cdaw.gsfc.nasa.gov/CME_list/`

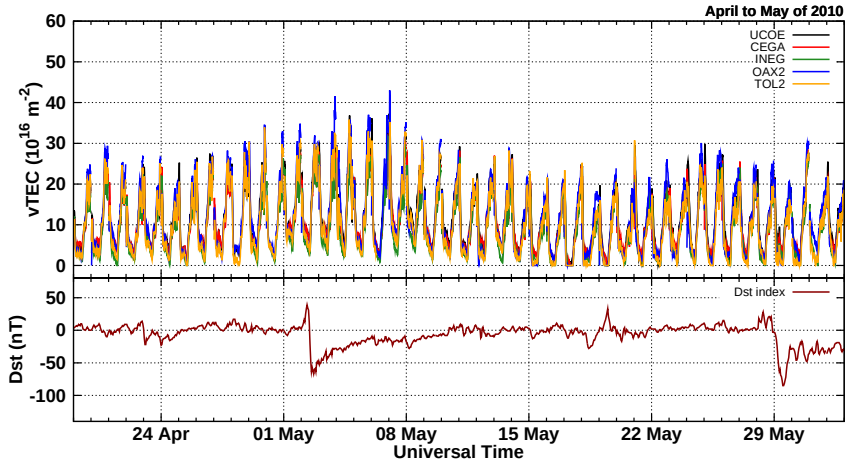

Figure 2 The vertical total electron content (*vTEC*) and *Dst* index. The top panel shows the *vTEC* calculated from five stations: UCOE, CEGA, INEG, OAX2 and TOL2, represented with lines in black, red, green, blue and orange colors respectively (see section 2.1). The bottom panel shows the *Dst* index. Both, *vTEC* and *Dst* index, are shown in the time interval from April to May 2010.

the interplanetary medium, and possibly along the line of sight between the radio sources and the MEXART observatory.

Four slow and narrow CMEs were observed on 29 April, which could be associated with the minimum on 2 May; however, these CMEs seemed to have no significant effect on the Earth's magnetosphere. The CMEs occurred at 01:12 UT, 03:36 UT, 07:00 UT, and 17:00 UT, and had velocities of 138 km s^{-1}, 178 km s^{-1}, 187 km s^{-1}, and 378 km s^{-1}, respectively. Their position angles (PAs) were around 80° for the first three, and 260° for the last one. All these CMEs seemed to originate from active region 11063 (N16 E11), very close to central meridian.

A coronal hole was observed in X-ray images obtained with satellite *GOES* 14 by the on of 24 April. This coronal hole appeared as a small region at the pole to the North–East of the solar disk. The coronal hole displaced towards the North–West during several days and reached lower latitudes where it became bigger. The high speed streams (∼600 to 700 km s^{-1}) originating in the coronal hole were registered by the plasma instruments onboard *Wind* and the *Advanced Composition Explorer* (ACE) from 30 April to 2 May 2010. Before the initiation of the geomagnetic storm, the solar-wind speed had an average value of ∼400 km s^{-1}. However, on 2 May, this value increased to around 650 km s^{-1}. This fact coincides with the growth of the plasma temperature (reaching 7×10^5 K). The magnetic field magnitude also showed an increase, which is consistent with an observed rotation of the southward component of the magnetic field, B_z and with the growth of the plasma pressure. Finally, the plasma *beta* parameter exhibited small values (close to zero) in the same time interval, confirming the effect of the high speed stream from this coronal hole.

Regarding the second minimum in the Dst index on 29 May, the active region 11072 (S15 W11) displayed some activity during several days starting on 24 May. A halo CME, with a linear speed of 427 km s^{-1} occurred on 24 May at ≈ 14:06

UT. X-ray images from *GOES* 14 also showed a coronal hole by the end of 24 May; it appeared as a small region at the pole to the North–East of the solar disk. This structure continuously moved to lower latitudes and became bigger. Thus, the presence of the active region, the CMEs occurrence, and the high speed stream from a coronal hole, which displayed the characteristics of a magnetic cloud (with a nice B_z rotation), may have led to the dip in *Dst* index. The *vTEC* showed a slight response to these events, whereas the *Dst* index presented minima. The total electron content had a maximum no greater than 45 *TECu* between 3 to 6 May, and no greater than 35 *TECu* between 29 and 31 May. Unfortunately, we do not have MEXART data for the period of 1 to 7 May. Depending on the availability of MEXART observations, we estimated the scintillation index for each source as in Pérez-Enríquez, Carrillo and Rodríguez (2006).

3.2 Wavelet Analysis

A wavelet transform can map the power of a particular frequency at different times, giving an expansion of the signal in both time and frequency. Furthermore, the wavelet transform not only tells us which frequencies can exist in the signal, but also shows whether a particular scale varies in time. In addition, the wavelet tool has an important advantage over Fourier transforms since it can extract frequency information from a signal using search windows of variable scales.

The wavelet analysis used in this work is based mainly on the wavelet software provided by C. Torrence and G. Compo[5], and programmed in the Interactive Data Language (IDL). We also included several new routines adapted to this software for analyzing MEXART data. These routines were developed to read the data and fitting gaussian functions to get a detrended time-series, which was used in our wavelet approach.

The wavelet analysis was applied to the radio signal of every source day by day to look for fluctuations that stand above the background signal along the time interval for the data analysis used in this work. With this tool we characterized the frequencies associated with these fluctuations in perturbed time subintervals (where the *Dst* geomagnetic index and TEC were slightly perturbed) and we compared them with undisturbed subintervals.

Figures 3 to 8 show wavelet plots for representative dates and sources. Each figure considers 4-day observations for one source. From top to bottom and from left to right we present in the first two panels, the time series together with a gaussian fitting (thick yellow line) and the amplitude of the detrended time-series below. In addition, the middle panels show the wavelet of the detrended time-series depicting the periodicities associated with the observations. The black lines indicate the influence of the cone region at a 95% significance level. To the right, the wavelet window shows the spectral power-spectrum highlighting the periodicities/frequencies above a line which represents the 95% significance level. Finally, the bottom panel shows the average variance.

Table 3 shows the best gaussian-fit parameters applied to the radio data in order to obtain a detrended signal. We selected representative dates for perturbed (*i.e.* 24 to 31 May) and unperturbed (*i.e.* 24 to 30 April and 13 to 18 May time

[5] http://atoc.colorado.edu/research/wavelets/

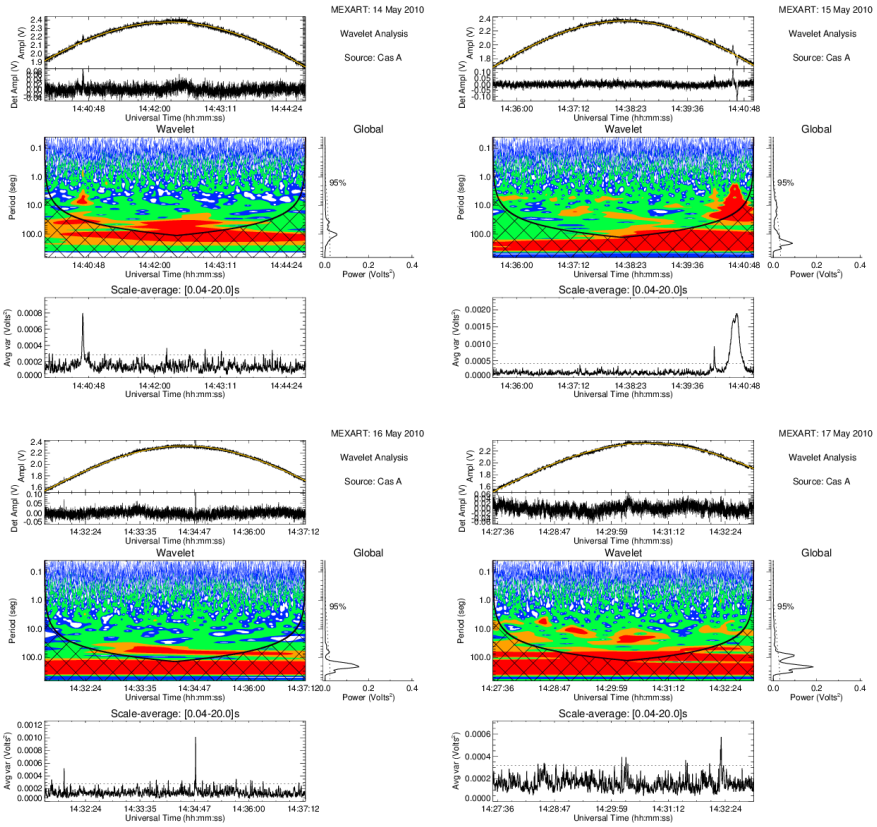

Figure 3 Wavelet analysis for the radio source Cas A, from 14 to 17 May. The radio signal of this source does not show significant disturbances during these days. These are characteristic wavelet-spectra of quiet days for this particular source. The level colors (black to red) for the power of each spectrum were: [0.0001, 0.0006, 0.007, 0.02, 0.5, 0.8, 2.0] V^2. See Section 3.2 for the explanation of every panel in this figure.

intervals) TEC for every source that reflects this behavior in several parameters. Table 3 also contains signal to noise ratio (S/N) values in the second column, the amplitude (A) in volts in the third column, the transit time (T.T.) recorded by the MEXART observatory for every source, the full-width at half-maximum (FWHM) in minutes, and the standard error between the fit and the radio signal, shown in the fourth, fifth, and sixth columns, respectively. The S/N ratio for the sources presented in this work took values between 4.1 to 36.8 (see Table 3), showing that the parameters obtained in our analysis were well determined.

Table 3: Parameters for the best fit to the radio signal obtained from the wavelet analysis, where S/N is the signal to noise ratio, A is the amplitude for each radio signal, T.T. is the transit time for each source, FWHM is the full-width at half-maximum, and E_{std} is the standard error between the fit and the signal-data.

Date	S/N	A (Volts)	T.T. (hr)	FWHM (min)	E_{std}

		Source: Cas A			
24 Apr. 2010	22.0	2.35	16.01	8.23	0.03
26 Apr. 2010	10.4	2.36	15.88	8.33	0.03
27 Apr. 2010	11.1	2.79	15.82	7.15	0.03
28 Apr. 2010	7.0	3.18	15.74	6.92	0.03
14 May 2010	14.3	2.38	14.70	8.13	0.01
15 May 2010	10.6	2.34	14.64	8.03	0.02
16 May 2010	9.4	2.32	14.58	8.04	0.01
17 May 2010	9.4	2.33	14.51	8.23	0.02
		Source: 3C405			
25 Apr. 2010	19.5	3.07	12.55	8.03	0.01
26 Apr. 2010	14.8	2.89	12.49	8.23	0.02
27 Apr. 2010	29.6	1.12	12.43	10.25	0.01
28 Apr. 2010	9.0	3.47	12.37	6.04	0.02
28 May 2010	22.8	2.46	10.41	10.34	0.02
29 May 2010	10.1	3.00	10.33	7.89	0.05
30 May 2010	30.6	2.49	10.28	11.98	0.01
31 May 2010	29.4	2.51	10.21	11.17	0.01
		Source: 3C144			
22 Apr. 2010	12.5	0.93	22.32	5.68	0.01
23 Apr. 2010	12.4	0.93	22.26	5.61	0.01
24 Apr. 2010	9.2	0.79	22.19	5.53	0.01
25 Apr. 2010	8.4	0.86	22.12	5.85	0.01
28 May 2010	6.2	0.74	19.96	5.26	0.02
29 May 2010	10.4	0.43	19.91	8.04	0.02
30 May 2010	11.1	0.42	19.85	8.54	0.01
31 May 2010	8.9	0.79	19.77	5.41	0.02
		Source: 3C48			
22 Apr. 2010	33.9	0.69	18.39	21.81	0.02
24 Apr. 2010	27.1	0.58	18.24	16.56	0.02
25 Apr. 2010	27.0	0.55	18.17	16.80	0.02
26 Apr. 2010	31.9	0.61	18.12	17.22	0.02
26 May 2010	21.2	0.37	16.14	11.69	0.02
28 May 2010	30.7	0.58	16.01	16.09	0.01
29 May 2010	36.8	0.62	15.95	16.63	0.01
30 May 2010	23.4	0.41	15.87	14.86	0.01
		Source: 3C274			
23 Apr. 2010	4.1	0.27	5.23	4.51	0.01
24 Apr. 2010	5.5	0.30	5.16	5.48	0.01
25 Apr. 2010	4.7	0.24	5.10	4.65	0.01
26 Apr. 2010	6.8	0.26	5.03	4.19	0.01
14 May 2010	4.8	0.27	3.85	4.66	0.01
15 May 2010	7.5	0.26	3.79	4.13	0.01
16 May 2010	5.1	0.25	3.72	4.42	0.01
17 May 2010	9.2	0.27	3.65	4.51	0.02
		Source: Cen A			
23 Abr. 2010	9.2	0.91	6.14	7.44	0.03
24 Abr. 2010	13.8	0.92	6.07	7.66	0.02

25 Abr. 2010	14.2	0.88	6.00	7.41	0.01
26 Abr. 2010	15.0	0.86	5.94	7.11	0.01
28 May 2010	14.3	0.78	3.84	7.16	0.02
29 May 2010	9.7	0.70	3.78	6.35	0.01
30 May 2010	10.2	0.85	3.71	7.44	0.03
31 May 2010	15.1	0.78	3.64	7.19	0.03

4 Discussion

In this paper we compared the perturbations observed with the MEXART radio telescope and those in the *vTEC* and the *Dst* index for the periods of observation from 20 to 30 April and from 8 to 31 May. Several sources were found to scintillate and we analyzed in which cases the signals were contaminated by IOND (as was found by Carrillo-Vargas et al. (2012)). Figure 9 shows the G index computed as:

$$G = \left(\frac{\langle \Delta I(t)^2 \rangle}{\langle I(t) \rangle^2} \right)^{1/2}, \tag{2}$$

for each source plotted as a function of time (in days), where the source intensity at a given time is $I(t)$ and its fluctuation around the mean is $\Delta I(t)$. The fluctuation is defined as $\Delta I(t) = I(t) - \langle I(t) \rangle$ and the mean intensity of the source is defined as $I_0 \sim \langle I(t) \rangle$ (Pérez-Enríquez, Carrillo and Rodríguez, 2006). From panel a), we observe that the G index shows an increase on 26 April for the sources Cen A and 3C274. Since the *Dst* index and the *vTEC* correspond to quiet periods, this suggests that these fluctuations are probably associated with perturbations in the interplanetary medium producing IPS. Moreover, Cas A also presents an increase on 30 April, suggesting an ionospheric origin. From panel b), we observe along this time interval that the G index for source 3C405 has stronger peaks. Due to the position of this source, we consider that its radio-signal behavior is related to ionospheric disturbances around the auroral region.

We discuss the behavior of the signal of each source:

1. *Cas A* shows no significant fluctuations in an undisturbed period from 14 to 17 May, as shown in Figure 3. The behavior of the radio signal is very similar for several days. Additionally, the wavelet analysis shows no significant periodicities/frequencies within the cone of influence for each day. This is in agreement with the observed power spectra, which show similar behaviors with no significant periodicities beyond a 95% significance level. Furthermore, we observe that sometimes there are narrow peaks mounted on the source radio-signal that modify the variance substantially (bottom panel). These peaks are associated with lightning storms close to the MEXART observatory and/or with transiting-satellite signals. We assume that these signals do not affect our analysis in a first approach, because they occur sporadically and randomly and do not affect substantially the periodicities and the power spectra. On the other hand, Figure 4 shows significant differences in the period 27 to 30 May in comparison with Figure 3. For instance, this radio source shows appreciable fluctuations on 27 May, when periods of ≈ 6 sec (≈ 0.17 Hz) and also ≈ 40 sec (≈ 0.025 Hz) are within the cone of influence. The behavior of the *vTEC* and

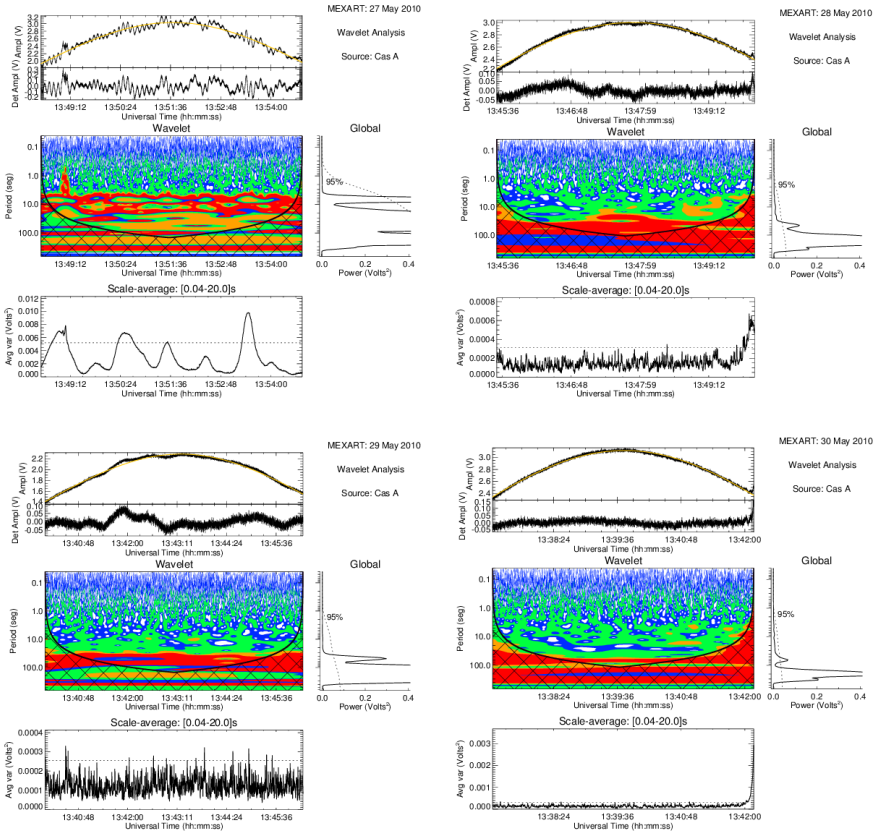

Figure 4 Wavelet analysis for the radio source Cas A, from 27 to 30 May. The fluctuations observed on 27 May could be associated with perturbations in the IPM producing IPS and, similarly, or 28 to 29 May. This source shows slight fluctuations in the signal related to a CME-Halo event (see Section 3). The level colors are the same as in Figure 3. See Section 3.2 for the explanation of every panel in this figure.

the *Dst* Index correspond to a quiet period for this day suggesting that these fluctuations are probably associated with ionospheric perturbations restricted to the auroral zone. In fact, on 28 May the radio signal shows slight fluctuations with periodicities greater than $\sim$50 sec ($\sim$0.02 Hz), but on 29 May there was an increase in power that concentrated around 20 sec ($\sim$0.05 Hz). This increase could be probably associated with the arrival to Earth of a CME, as is reflected by the *Dst* index for these days. Several CMEs took place around this period, but we believe that only the halo CME observed ($\sim$14:06 UT, with a velocity of 427 km s^{-1}) on 24 May plus the high-speed stream from a coronal hole observed on the solar disc may be responsible for the geomagnetic storm (see Figure 2). In this scenario, a complete study is always useful to understand the whole context in the interplanetary medium, interplanetary CMEs (*e.g.*, ejecta and magnetic cloud), corotating interaction regions or CIRs, etc. Finally, on 30 May the behavior of this source radio-signal returns to a quiet state without fluctuations, as shown in Figure 4. Figure 5 shows a different

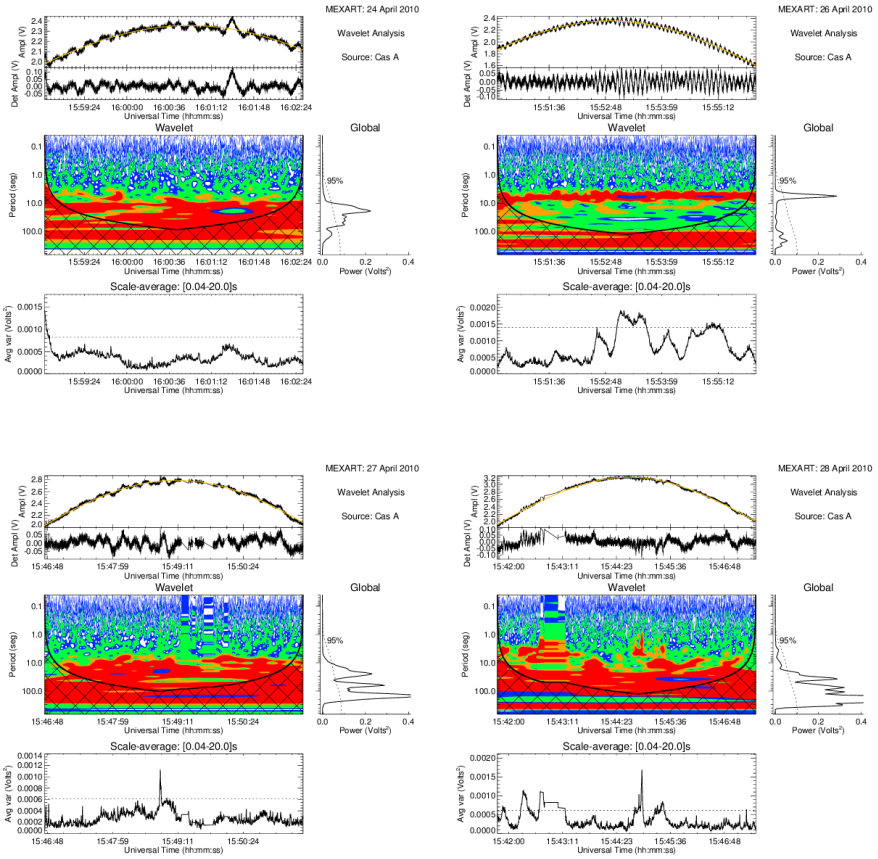

Figure 5 Wavelet analysis for the radio source Cas A from 24 to 28 April. For all of these days, Cas A shows clear and different fluctuations. On 24 and 26 April, these fluctuations may be due to perturbations in the IPM producing IPS; however, on 27 and 28 April, the fluctuations may be associated with IPS and IOND. The level colors are the same as in Figure 3. See Section 3.2 for the explanation of every panel in this figure.

period of observation for this source, from 24 to 28 April. During this period of time, the radio signal presents fluctuations every day. However, the frequencies indicate different origins. In fact, for 24 and 26 Arpil the *vTEC* and the *Dst* index display a behavior corresponding to a quiet period (see Figure 2), suggesting that these fluctuations are probably associated with perturbations in the interplanetary medium producing IPS. For 27 and 28 April, the fluctuations could be associated with IPS plus IOND. Figure 9 shows that the index presents an abrupt peak on 30 April. This increase, although due to ionospheric disturbances, as can be appreciated from the wavelet analysis, does not let us clearly understand what is the contribution of the ionosphere (in relation with the *Dst* variation) because this requires data from more radio sources.

2. *3C405* shows a behavior similar to that of *Cas A*, when on 28 May the radio signal presents slight fluctuations with periodicities greater than 50 sec (∼0.02 Hz) and with a significant power at these frequencies. However, on 29 May, the fluctuations are stronger with periodicities greater than 10 sec (∼0.1 Hz) and also

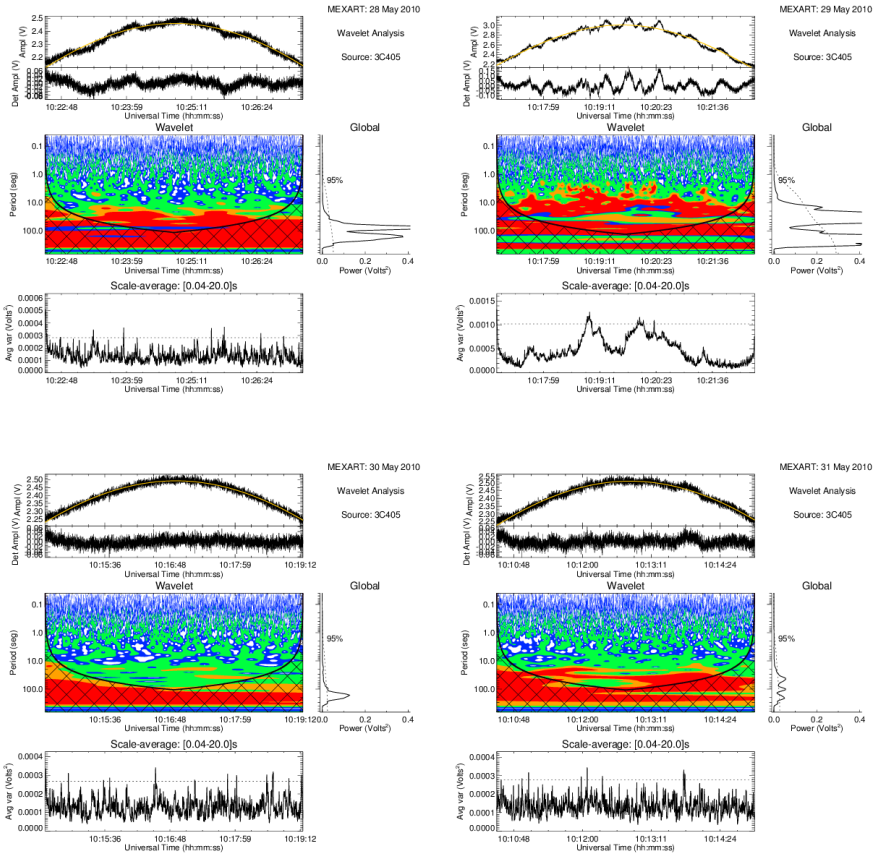

Figure 6 Wavelet analysis for the radio source 3C405 from 28 to 31 May. This source shows strong fluctuations on 29 May, probably associated with IPS (see Section 4). The level colors are the same as in Figure 3. See Section 3.2 for the explanation of every panel in this figure.

with a significant power at these frequencies (see Figure 6). Because the *vTEC* (see Figure 10) is not highly altered locally on 29 May, it is suggested that the fluctuations observed are probably due to ionospheric perturbations around the auroral region. On 30 May the radio signal of this source shows a behavior corresponding to a quiet period. Finally, on 31 May, the radio signal of this source presents slight fluctuations: however, in this case, the *vTEC* (see Figure 10) is also slightly perturbed at the end of 30 May, suggesting that the observed fluctuations may be contaminated by ionospheric disturbances (see Figure 6).

3. *3C144* shows a different behavior. No fluctuations were observed on 27 May (see Figure 7). However, the radio signal of this source is highly perturbed, the perturbations have periods of around 10 sec (∼0.1 Hz). In addition, both the *vTEC* and the *Dst* (see Figure 10) show a behavior typical of quiet periods, suggesting that the fluctuations observed on this day may be due to IPS. There are several CME events between 25 and 28 May that may contribute to the IPS. Finally, on 29 and 30 May no significant fluctuations are observed (see Figure 7).

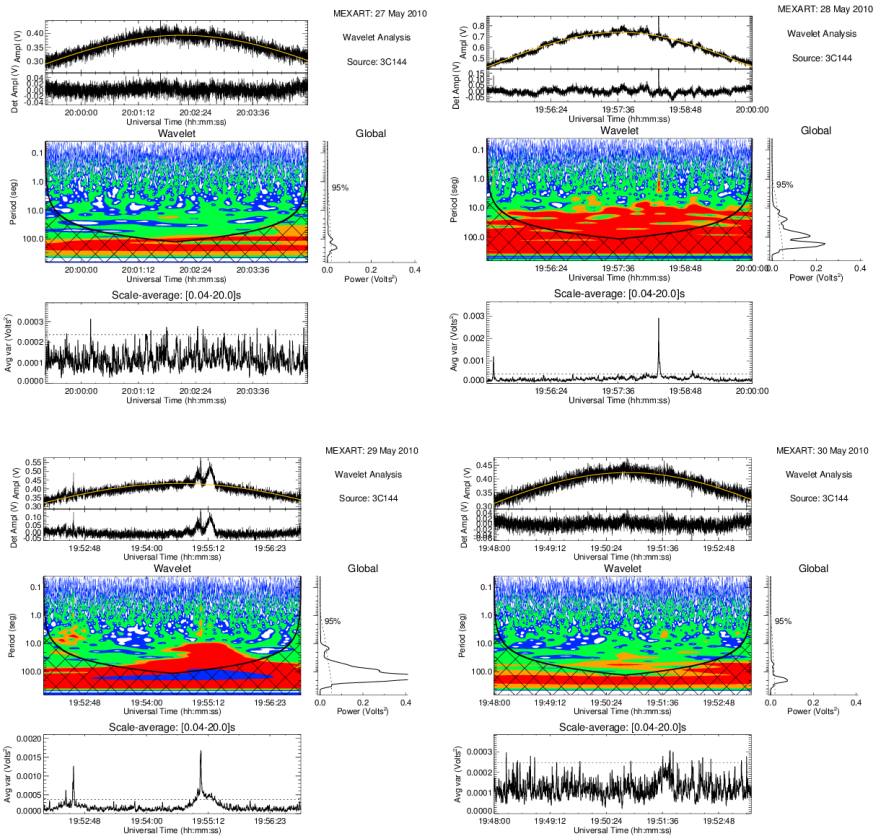

Figure 7 Wavelet analysis for the radio source 3C144, from 27 to 30 May (see Section 4). The level colors are the same as in Figure 3. See Section 3.2 for the explanation of every panel in this figure.

4. *3C48,* remains unperturbed on 26 and 30 May, but on 28 and 29 May there are slight fluctuations observed in the wavelet window. However, the power spectra show no periodicities above the 95% significance level (see Figure 8). In this case, the fluctuations observed could be associated with IPS and ionospheric perturbations, respectively. However, we need a higher S/N to have a better definition of their origin.

In summary, we have observed several sources that present fluctuations in their radio signal (see Table 1). These fluctuations may be associated with IOND, suggested by the *vTEC* in some days; but, in other cases, they were associated with IPS, and sometimes with both. The fact that sometimes the radio signal from astronomical sources is contamined by ionospheric disturbances, suggests that these fluctuations should be taken into account as possible sources of contamination in IPS measurements obtained with the MEXART observatory (Carrillo-Vargas et al., 2012).

From our results, we have found that this complementary study can help to understand the origin of the observed fluctuations in the radio signal of astronomical

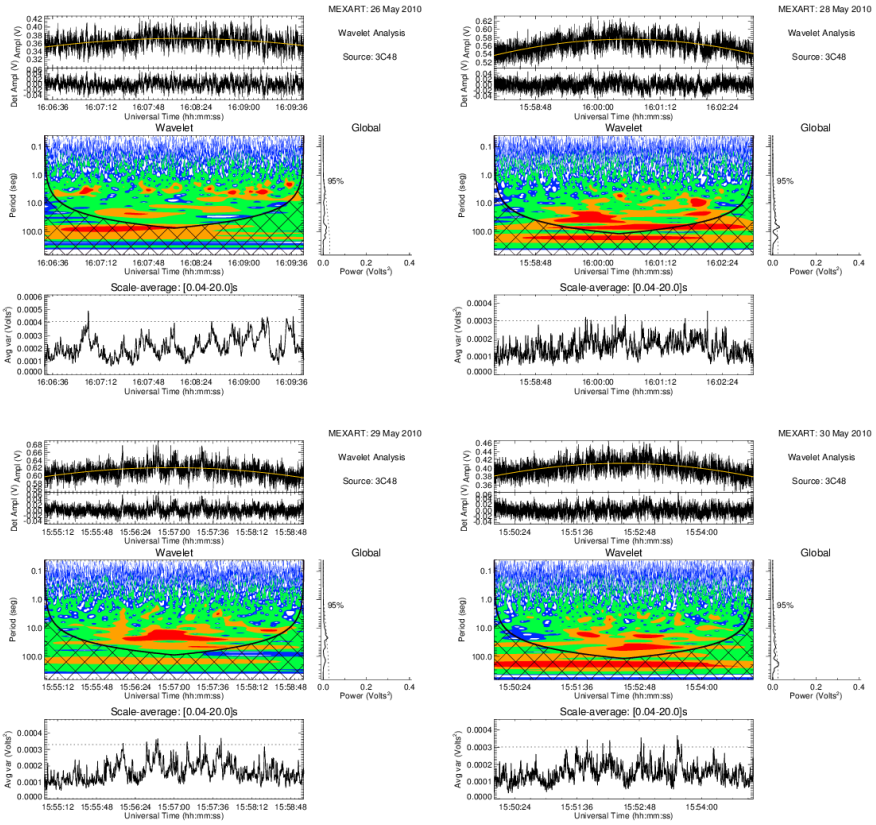

Figure 8 Wavelet analysis for the radio source 3C48 from 26 to 30 May (see Section 4). The level colors are the same as in Figure 3. See Section 3.2 for the explanation of every panel in this figure.

sources. In addition, we have found that the ionospheric disturbances can play an important role in the contamination of the signal when looking for IPS. The ionosphere acts as an obstacle to radio waves of ≤ 150 MHz (Cohen and Röttgering, 2009) and sometimes it is not possible to discriminate *a priori* between IPS or ionospheric disturbances as sources of the observed intensity fluctuations recorded by MEXART.

From a further analysis using the radio signal from satellites transiting close to an astronomical source and detected by MEXART observatory, it was possible to discern whether the intensity fluctuations were associated with IOND or IPS (Carrillo-Vargas et al., 2012). In this context, we have used an additional tool, a wavelet analysis, in this article. This alternative tool lets us characterize the perturbed signal.

5 Conclusions

The conclusions of our work can be summarized as follows:

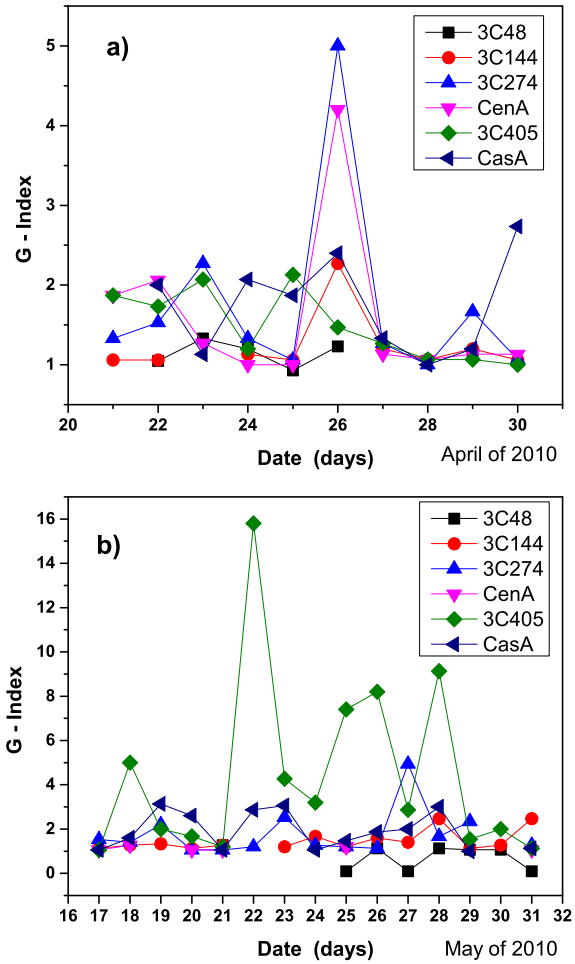

Figure 9 The G-index, as defined in Pérez-Enríquez, Carrillo and Rodríguez (2006), is plotted as a function of time (in days). Panel a) shows the behavior for each radio source used in our analysis from 21 to 30 of April, close to the time of the first *Dst* minimum on 2 May. On 26 April, 3C274 and Cen A exhibit a significative G-index, its value was twice large than for others sources. Panel b) shows the same data as panel a), but from 16 to 31 May. The source 3C405 shows several peaks indicating a high G-index along the line of sight (see the text for more details in section 4).

– Our study incorporates the use of wavelets together with complementary information provided by the *vTEC* and *Dst* index. This is the first time these tools have been applied to MEXART data and allow a better understanding of cases when the IPS may be contaminated by IOND.
– Within the period of April–May 2010, several radio sources presented fluctuations in their radio signal registered with the MEXART. Using wavelets we found the periods/frequencies that characterize these fluctuations. We found that the perturbations in the signal were sometimes associated with IOND and/or IPS (see for instance Figure 4 top left, Figure 5 top left and Figure 8

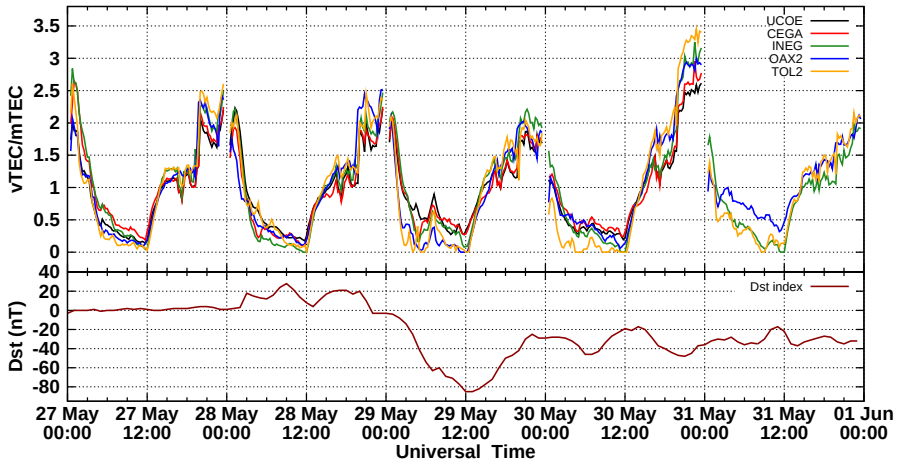

Figure 10 The vertical total electron content (*vTEC*) and *Dst* and the Dst index shown in detail from 27 May to 1 June 2010. The top panel shows the *vTEC* divided by the mean value of the TEC (mTEC) and calculated using data from five stations: UCOE, CEGA, INEG, OAX2 and TOL2, represented with lines in black, red, green, blue and orange colors respectively (see section 2.1). The bottom panel shows the *Dst* index.

top right). In this context the *vTEC* can help to establish the cases in which the IPS is actually contaminated by IOND. Furthermore, in the example shown in Figure 8 (top left), the wavelet analysis indicates that the ionospheric scintillation is associated with quiet conditions, and in Figure 5 (top left) and Figure 6 (top right) the wavelet analysis shows ionospheric disturbances associated with the geomagnetic storm.

- In addition, Fourier spectra show that these fluctuations have frequencies between $\sim$0.01 Hz to $\sim$1.0 Hz (periods of 100 sec to 1 sec, respectively) for both IOND and IPS. We found that there is a tendency for the frequencies close to $\sim$1.0 Hz to be more likely associated with IPS, whereas lower frequencies tend to be related to IOND. However, in the cases where both IPS and IOND occur, we could not distinguish between them.
- In the examples that neither the Dst index nor the *vTEC* showed any significant change, we can say that the fluctuations are not related to global ionospheric effects but could be probably related to IPS. We observed that when the *vTEC* is perturbed and solar-origin effects can be assumed, then the radio signal can be contaminated by ionospheric perturbations. This is probably the case observed by Carrillo-Vargas et al. (2012), where the fluctuations could be attributed to IOND and/or IPS.
- The solar-minimum period has allowed us to characterize better the radio fluctuations of astronomical sources observed with the MEXART, during this period the ionosphere can contribute strongly. This is especially true for those sources that having large elongations (around 90°, for instance) present fluctuations in their signal. However, more work is needed to characterize the intrinsic fluctuations in the radio signal.

Acknowledgements The authors thank the MEXART team, in particular: A. González-Esparza (P. I. of MEXART), P. Villanueva, E. Andrade, and E. Aguilar, for the technical support and provision of data. We also thank CORS, SOPAC and UNAVCO for incorporating the data on their respective websites from which the GPS data can be freely downloaded. We are also grateful to NOAA-SWPC for access to the TEC calculation program. We also wish to thank the Servicio Sismológico Nacional and E. Cabral for providing some Mexican GPS data. This article was possible thanks to the PAPIIT-UNAM projects IN111509 and IA102514-2. M. Rodríguez-Martínez also thanks REDCyTE and CONACyT for a postdoctoral fellowship supported by the project *Estudio de la ionosfera y sus aplicaciones* for the Mexican Space Agency (MSA). The authors finally thank the suggestions of M. Sánchez and S. Kurtz that have improved this article.

References

Araujo-Pradere, E. A.: 2005, GPS-derived total electron content response for the Bastille Day magnetic storm of 2000 at a low mid-latitude station. *Geofis. Int.* **44**, 211.

Araujo-Pradere, E.A., Fuller-Rowell, T.J., Spencer, P.S.J.: 2006, Consistent features of TEC changes during ionospheric storms. *J. Atmos. Solar-Terr. Phys.* **68**, 1834.

Carrillo-Vargas A., Pérez-Enríquez, H. R., Rodríguez-Martínez, M., López-Montes, R., Casillas-Pérez, G. A., Araujo-Pradere, E. A.: 2012, Ionospheric disturbances detected by MEXART. *Adv. Space Res.*, **49**, 11.

Carrillo-Vargas A.: 2007, Construcción y calibración del radiotelescopio de centelleo interplanetario MEXART. Ph.D. Thesis Univ. Nacional Autónoma de México.

Cohen, A. S., Röttgering, H. J. A.: 2009, Probing Fine-Scale Ionospheric Structure with the Very Large Array Radio Telescope. *Astron. J.* **138**, 439.

Erickson, W. C., Perley, R. A., Flatters, C., Kassim, N. E.: 2001, Ionospheric corrections for VLA observations using Local GPS data. *Astron. Astrophys.* **366**, 1071.

Gapper, G. R., Hewish, A., Purvis, A., Duffett-Smith, P. J.: 1982, Observing interplanetary disturbances from the ground. *Nature.* **296**, 633.

González-Esparza, J. A., Carrillo A., Andrade E., Pérez-Enríquez R., Kurtz S.: 2004, The MEXART interplanetary scintillation array in Mexico. *Geofis. Int.* **43**, 61.

González-Esparza, J. A., Carrillo, A., Andrade, E., Sierra, P., Vazquez, S., Rodríguez, C., Pérez-Enríquez, R., Kurtz, S., Blanco-Cano, X.: 2006, Calibration and testing of the MEXART antenna using solar transits. *Adv. Space Res.* **38**, 1824.

Hewish, A., Bravo, S.: 1986, The sources of large-scale heliospheric disturbances. *Solar Phys.* **106**, 185.

Hewish, A., Duffet-Smith, P. J.: 1987, A new method of forecasting geomagnetic activity and proton showers. *Planet Space Sci.* **35**, 487.

Hewish, A., Scott, P. F., Wills, D.: 1964, Interplanetary Scintillation of Small Diameter Radio Sources. *Nature* **203**, 1214.

Jackson, B. V., Hick, P. L., Kojima, M., Yokobe, A. 1998, Heliospheric tomography using interplanetary scintillation observations 1. Combined Nagoya and Cambridge data. *J. Geophys. Res.* **103**, 12049.

Komjathy, A.: 1997, Global ionospheric total electron content mapping using the Global Positioning System. Technical Report No. 188, New Brunswick. Ph.D. Thesis Univ. of New Brunswick.

Langley, R. B.: 1996, Propagation of the GPS signals. Lec. Notes Earth Sci., **60**, 103.

López-Montes, R., Pérez-Enríquez, R., Araujo-Pradere, E. A.: 2012, The impact of large solar events on the total electron content of the ionosphere at mid latitudes. *Adv. Space Res.*, **49**, 7, 1167.

Lucek, E. A., Clark, T. D. G., Moore, V.: 1996, The use of various interplanetary scintillation indices within geomagnetic forecasts. *Ann. Geophys.* **14**, 139.

Manoharan, P.K.: 2010, Evolution of Near-Sun Solar Wind Turbulence. In: Hasann, S.S.,Rutten, R.J.(eds.),*Magnetic Coupling between the Interior and Atmosphere of the Sun,Astrophys. Space Sci. Proc.* **XII**, Springer, Dordrecht, 324.

Manoharan, P. K., Ananthakrishnan, S.: 1990, Determination of solar-wind velocities using single-station measurements of interplanetary scintillation. *Month. Not. Roy. Astron. Soc.* **244**, 691.

Manoharan, P.K., Kojima, M., Misawa, H.: 1994, *J. Geophys. Res.* **99**, 23411.

Milne, R.G.: 1976, *Aust. J. Phys.* **29**, 201.

Mejia-Ambriz, J. C., Villanueva-Hernandez, P., Gonzalez-Esparza, J. A., Aguilar-Rodriguez, E., Jeyakumar, S.: 2010, Observations of Interplanetary Scintillation (IPS) Using the Mexican Array Radio Telescope (MEXART). *Solar Phys.* **265**, 309.

Pérez-Enríquez, R., Carrillo, A., Kotsarenko, A., Cruz-Abeyro, J. A. L.: 2008, State of the inner heliosphere as given by the G index of interplanetary scintillation and the *Dst* index of geomagnetic activity. *J. Geophys. Res.* **113**, 10107.

Pérez-Enríquez, R., Carrillo, A., Rodríguez, C.: 2006, Fractal character of G-index of IPS data for the period 1991-1994 obtained from multiscale wavelet analysis. *Adv. Space Res.* **38**, 1819.

Purvis, A., Tappin, S. J., Rees, W. G., Hewish, A., Duffett-Smith, P. J.: 1987, The Cambridge IPS survey at 81.5 MHz. *Month. Not. Roy. Astron. Soc.* **229**, 589.

Shishov, V. I., Tyul'Bashev, S. A., Chashei, I. V., Subaev, I. A., Lapaev, K. A.: 2010, Interplanetary and Ionosphere Scintillation Monitoring of Radio Sources Ensemble at the Solar Activity Minimum. *Solar Phys.* **265**, 277.

Tappin, S. J., Hewish, A., Gapper, G. R.: 1984, Tracking a high-latitude corotating stream for more than half a solar rotation. *Planet. Space Sci.* **32**, 1273.

Tsurutani, B.T., Verkhoglyadova, O.P., Mannucci, A.J., Lakhina, G.S., Li, G., Zank, G.P.: 2009, *Radio Sci.* **44**, RS0A17.

Woan, G.: 1995, Observations of long-lived solar wind streams during 1990-1993. *Ann. Geophys.* **13**, 227.